Zhang *et al. Animal Diseases* (2026) 6:2
https://doi.org/10.1186/s44149-025-00205-7

Animal Diseases

CASE REPORT Open Access

Case report: Lumpy skin disease case analysis in central China

Junhao Zhang[1], Lei Kuang[1], Xue Qi[1], Yanting Du[1], Xinhuai Shi[1], Mingxuan Jiang[1], Chuanheng Jiang[1], Enpei Zheng[1], Ziyuan Weng[1], Ling Shi[1], Xinwei Yuan[1], Wanfeng Ji[1], Aizhen Guo[1,2,3,4], Jindong Gao[5*] and Changmin Hu[1*]

Abstract

Lumpy skin disease (LSD), a highly contagious viral infection caused by Lumpy Skin Disease Virus (LSDV), has caused severe economic losses. We analyzed three representative outbreaks in 2024, combining clinical, histopathological, serological, and molecular data to refine regional control strategies. According to our findings, affected cattle presented with generalized cutaneous nodules, fever and peripheral edema; one-third of in-contact animals remained clinically normal yet seroconverted within ten days. Antibody titers peaked at approximately 20 d post-onset and were accompanied by persistent viral DNA in saliva, ocular secretions and skin scabs. Histology revealed alveolar septal edema, hepatocellular ballooning, and glomerular necrosis, whereas biochemical profiling revealed hypalbuminemia, hyperglobulinemia, and elevated alanine aminotransferase in one patient. Immunohistochemistry revealed intense LSDV antigen in the spleen, alveolar septa of the lung, and throughout the dermis of the skin nodules, identifying these tissues as the most reliable diagnostic targets. The combined findings confirm active viral replication in cutaneous, respiratory and lymphoid tissues, highlight the occurrence of subclinical infection and underscore the value of paired serology and PCR for herd screening. Prompt isolation, vector control and vaccination with homologous capripox vaccines are recommended to curtail transmission and economic impact.

Keywords Lumpy skin disease virus, Pathology, Immunohistochemistry, Disease control and prevention

Introduction

Lumpy skin disease virus (LSDV), a double-stranded DNA virus classified under the genus Capripoxvirus of the family Poxviridae, primarily infects cattle. It shares protective antigens with phylogenetically related goat pox virus (GTPV) and sheep pox virus (SPPV), which enabled the historical application of GTPV vaccines for emergency immunization against LSD during early outbreaks (Tuppurainen et al. 2014; Davies 1976). However, SPPV-based vaccines demonstrate limited protective efficacy in LSDV-infected cattle (Ayelet et al. 2013). Mechanical transmission by hematophagous insects, particularly *Stomoxys* spp. and *Culicoides* midges, is regarded as the principal route of LSDV spread, and seasonal peaks coincide with high vector abundance. LSDV was first identified in Zambia in 1929 and subsequently spread through

Handling editor: Caihua Dong

*Correspondence:
Jindong Gao
gaovet@126.com
Changmin Hu
hcm@mail.hzau.edu.cn
[1] Department of Clinical Veterinary Medicine, College of Veterinary Medicine, Huazhong Agricultural University, Wuhan 430070, China
[2] Hubei Hongshan Laboratory, Wuhan 430070, China
[3] Cooperative Innovation Center for Sustainable Pig Production, Huazhong Agricultural University, Wuhan 430070, China
[4] Hubei International Scientific and Technological Cooperation Base of Veterinary Epidemiology, Wuhan 430070, China
[5] College of Animal Science and Technology, Tarim University, Alar 843300, China

sub-Saharan Africa, the Middle East and Europe before it reached Asia (Sendow et al. 2024; Parvin et al. 2022; Borm et al. 2023). Recent epidemiological surveillance has revealed persistent global dissemination of LSDV, particularly across Asian regions, including Kazakhstan, Mongolia, Russia, Thailand, and China (Shumilova et al. 2022; Sprygin et al. 2022; Sariya et al. 2022). Following its initial detection in Xinjiang, China (2019), the virus rapidly expanded to Inner Mongolia, Hong Kong, Yunnan, Shandong, and Guangdong (Flannery et al. 2021; Wang et al. 2022), and the present study investigates the clinical and pathological features of recent LSD outbreaks in Hubei and Anhui, quantifies serological and molecular dynamics, including virus distribution in tissues and secretions, and provides evidence-based guidance on vaccination and biosecurity measures for disease containment, correlating clinical signs with pathology, serology and PCR findings to refine regional containment strategies.

Case presentation

Background of the cases

Field monitoring conducted in Anhui and Hubei Provinces during the autumn season identified clinical manifestations of lumpy skin disease in cattle herds. The affected cattle presented with an acute onset of high fever, lethargy, and anorexia. Cutaneous nodules appeared on the body surface (Fig. 1A), and ruptured vesicles on the muzzle developed into dark, hardened lesions (Fig. 1B). Additionally, some animals exhibited limb edema (Fig. 1C). In certain cases, the condition progresses to ulcerative nodules accompanied by secondary infections and purulent exudation. Prolonged anorexia resulted in progressive weight loss among the clinically affected cattle.

As the disease advanced in certain affected cattle, there was a noticeable exacerbation of emaciation and a decline in appetite. Despite the administration of supportive care, which includes fluid therapy and anti-inflammatory medications, the vital signs of some animals continue to deteriorate. An examination of herd records preceding the outbreak revealed an absence of history of vaccination against goatpox or lumpy skin disease virus and no recent introduction of new cattle into the herd.

Sample collection

Whole blood samples and selected tissues were collected aseptically from patients with clinically confirmed lumpy skin disease. In a subset of additional confirmed animals, the sampling protocol included whole blood together with cardiac, hepatic, splenic, pulmonary, and renal tissues and cutaneous nodules. All the samples were transferred into sterile, prelabeled containers, chilled on wet ice and processed within four hours for serological, molecular and histopathological examinations.

Results of DNA and antibody tests

Polymerase chain reaction (PCR) analysis, which targeted a conserved 376 base pair region, confirmed the presence of LSDV DNA in dermal scabs and mucosal secretions collected from clinically affected cattle. All the negative controls remained blank, confirming the specificity of the assay (Fig. 2A). Testing of 19 serum samples from 16 animals (three herds) for LSDV antibodies via an ELISA revealed a temporal dynamic of antibody production. A key finding was that no LSDV antibodies were detectable in the serum of affected animals within the first 7 d after clinical onset (Fig. 2B). Antibodies were subsequently detected, with a marked increase observed in three individuals with longitudinal data. An investigation also revealed antibody-positive cases that lacked clinical signs. These findings collectively confirm exposure within herds and highlight the importance of considering the seroconversion window in outbreak investigations.

Pathological changes

The gross necropsy findings indicated that the pathological manifestations were predominantly confined to

Fig. 1 Clinical spectrum of lumpy skin disease observed during the 2024 outbreak. **A** Extensive nodules appear on the skin all over the body of the affected dairy cattle. **B** Discrete pox-like lesion on the nasal planum (green arrow). **C** Right forelimb distal edema (red arrow)

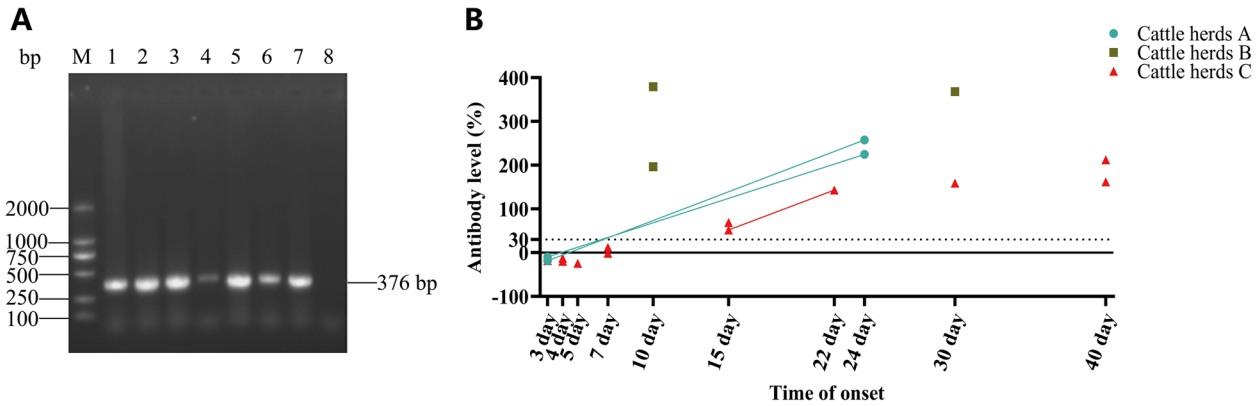

Fig. 2 Integrated molecular and serological evidence of lumpy skin disease virus infection. **A** Conventional PCR amplification of a 376 bp viral ORF from representative clinical samples. Lane M, molecular weight marker; lanes 1–6, lesion or secretion samples; lane 7, positive control; lane 8, negative control. **B** Antibody kinetics following LSDV infection across three herds. Individual antibody levels (ELISA S/P ratio) from all 19 serum samples are plotted. Each symbol represents a single measurement. Symbols are shaped and colored by farm of origin (cattle herds A: circles, khaki; cattle herds B: squares, green; cattle herds C: triangles, red). Lines connect sequential measurements from the same animal ($n = 3$), illustrating individual longitudinal trajectories. Measurements from animals sampled only once ($n = 13$) are shown as unconnected symbols. The total number of samples ($n = 19$) reflects 16 unique animals, with three animals contributing two time points each. The dashed horizontal line indicates the ELISA positive cutoff

the pulmonary system. A nodule, approximately three centimeters in diameter, was identified in the right lung (Fig. 3A, red circle). This mass was characterized by its firm texture, well-defined margins, and resistance to compression, which are indicative of chronic granulomatous inflammation with fibrous encapsulation. The adjacent lung parenchyma exhibited patchy dark red consolidation and diffuse vascular injection, suggesting compromised perfusion and alveolar collapse in the surrounding tissue.

All other organs appeared normal upon macroscopic examination. The bifurcated uterus was uniformly flaccid

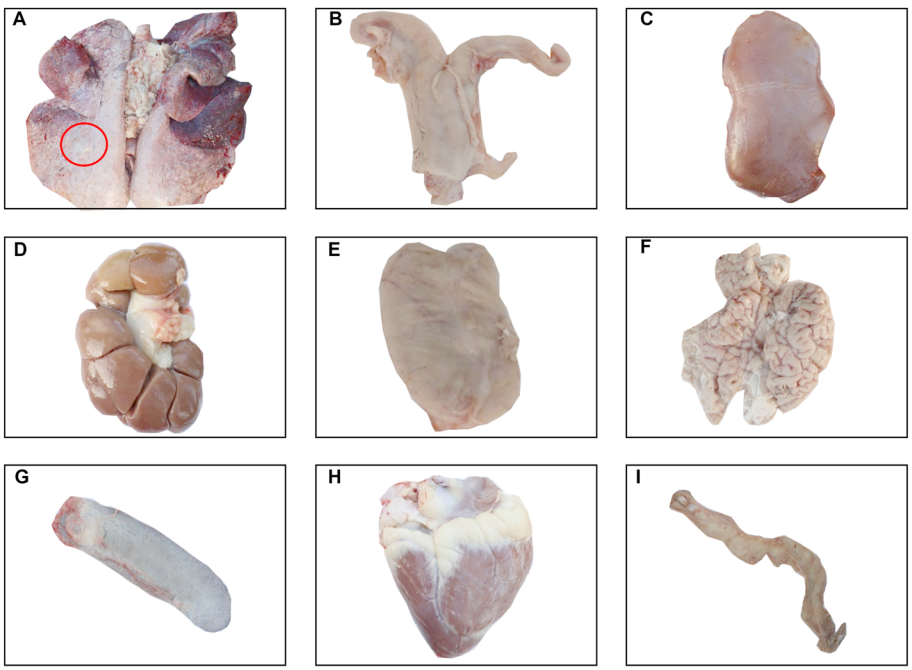

Fig. 3 Gross morphology of visceral organs from cattle with lumpy skin disease. **A** Lung with a red circle indicating a focal lesion. **B** Uterus. **C** Liver. **D** Kidney. **E** Urinary bladder. **F** Brain. **G** Spleen. **H** Heart. **I** Small intestine

without any serosal fibrin or endometrial discoloration and appeared unremarkable with no significant lesions (Fig. 3B). The liver maintained a smooth capsule and consistent coloration, exhibiting no gross pathological changes (Fig. 3C). The kidneys displayed normal reniculate architecture and coloration, and the capsules were easily detachable, supporting the absence of overt nephrosis despite subsequent evidence of glomerular injury (Fig. 3D). The urinary bladder wall was translucent and avascular, without vascular congestion, and showed no notable abnormalities, effectively ruling out cystitis (Fig. 3E). The cerebral and cerebellar surfaces were intact and devoid of petechiae or malacia, demonstrating preserved gyral architecture and the absence of surface hemorrhage (Fig. 3F). The spleen demonstrated only mild enlargement and presented a homogeneous cut surface with no evident lesions, which obscured the extensive presence of white-pulp viral antigens, as revealed by immunohistochemical analysis (Fig. 3G). The heart displayed a smooth epicardium devoid of pallor or ecchymoses, with an intact epicardium and maintained chamber geometry (Fig. 3H). The small intestinal segment exhibited smooth serosal and mucosal surfaces with minimal gas distension and appeared smooth and pliable with no significant pathological findings, suggesting that the alimentary tract was not a primary target of this infection (Fig. 3I).

Histopathological observations

Systemic pathological alterations were predominantly localized within the lungs, liver, kidney, and skin. In the liver, portal regions are broadened by infiltrating lymphocytes and macrophages, whereas peripheral hepatocytes exhibit marked ballooning degeneration. Amorphous eosinophilic amyloid deposits were observed compressing the sinusoidal channels, thereby disrupting the normal lobular architecture. The centrilobular areas further displayed sinusoidal congestion accompanied by hepatocellular loss (Fig. 4A). Pulmonary lesions are characterized by swollen alveolar septal cells and consequent collapse of the alveolar spaces. Notably, thrombus formation was identified within the lumina of arterioles (Fig. 4B, black square). Renal pathology involved glomerular focal necrosis. Specifically, in bovine sample C3, renal tubules presented significant dilation with epithelial attenuation, whereas adjacent tubules presented signs of compensatory epithelial hypertrophy (Fig. 4C). In the skin, the spectrum of injury evolved from early lesions showing prominent epidermal and adnexal hyperplasia through intermediate stages featuring full-thickness coagulative necrosis and obliteration of small dermal vessels to late-stage plaques exhibiting suprabasal vacuolar degeneration alongside dense dermal fibroplasia, indicative of ongoing reparative remodeling (Fig. 4D). Compared with that in normal skin regions, the lesional dermal layer was significantly thickened (Fig. 4D1), with

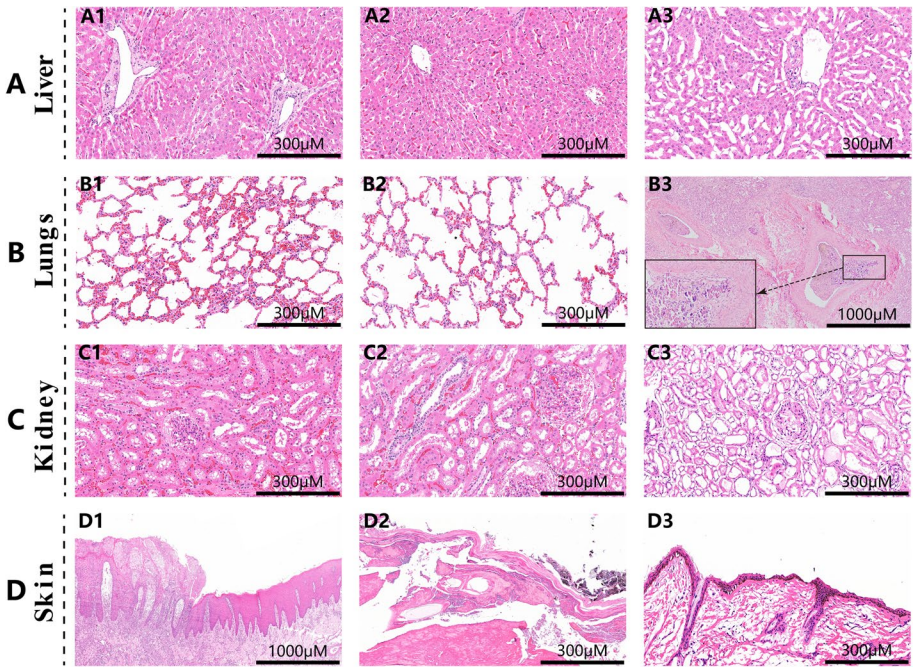

Fig. 4 Representative hematoxylin and eosin-stained sections of visceral organs and skin from cattle with lumpy skin disease. **A** Liver section. **B** Lung section; the black square highlights a specific area (B3). **C** Kidney section. **D** Skin sections at different stages

evident disruption of the normal epidermal structure and marked inflammatory cell infiltration. No significant pathological changes were observed in other organ systems.

Immunohistochemical observations

Immunolabeling for the LSDV protein revealed a strikingly coherent tissue-tropism profile. In the spleen, brown intracytoplasmic staining accumulated prominently at the interface between the white pulp follicles and the red pulp cords, indicating a high viral load within the antigen-presenting cells residing in this region (Fig. 5A). In pulmonary sections, viral antigens were observed decorating alveolar septal macrophages and type II pneumocytes. In more advanced lesions, the staining extended diffusely through the pulmonary interstitium, outlining the alveolar septa and confirming active viral replication in these cellular compartments (Fig. 5B). Cutaneous nodules presented the heaviest antigen burden, where intense immunolabeling was present in basal and suprabasal keratinocytes, perifollicular fibroblasts, and dermal macrophages. This created a continuous positive band extending from the epidermis to the deep reticular dermis, emphasizing the pronounced cutaneous tropism of the virus (Fig. 5C). According to the semi-quantitative scoring system based on the percentage of positive cells and staining intensity (Li et al. 2015), panels A1, A2, A3, and B1 in Fig. 5 were scored as +; B3, C2, and C3 as ++; and B2 and C1 as +++.The spatial concordance between viral antigen distribution and the sites of vascular injury highlighted an angiotropic predilection, which underpins the multifocal thrombotic pathology observed in hematoxylin and eosin-stained sections.

Serum biochemistry

Fourteen days after symptoms began, serum chemistry revealed two distinct patterns, indicating that lumpy skin disease has varying effects on liver function and lipid metabolism. The first pattern included low albumin (2.4 g/dL), high globulin (6.0 g/dL), and a low albumin–globulin ratio (0.4), with slightly elevated total protein (8.3 g/dL). The alanine aminotransferase level was high at 70 U/L, whereas other liver enzymes and bilirubin levels were normal. The cholesterol concentration was notably low at 27 mg/dL. These findings suggest mixed liver damage and acute-phase protein production, aligning with histological signs of liver cell damage and inflammation (Table 1).

We observed selective lipid dysregulation, with cholesterol reduced to 39 mg/dL, whereas protein metabolism, renal function, liver enzymes, and electrolytes remained normal. This isolated hypocholesterolemia suggests early or mild liver involvement

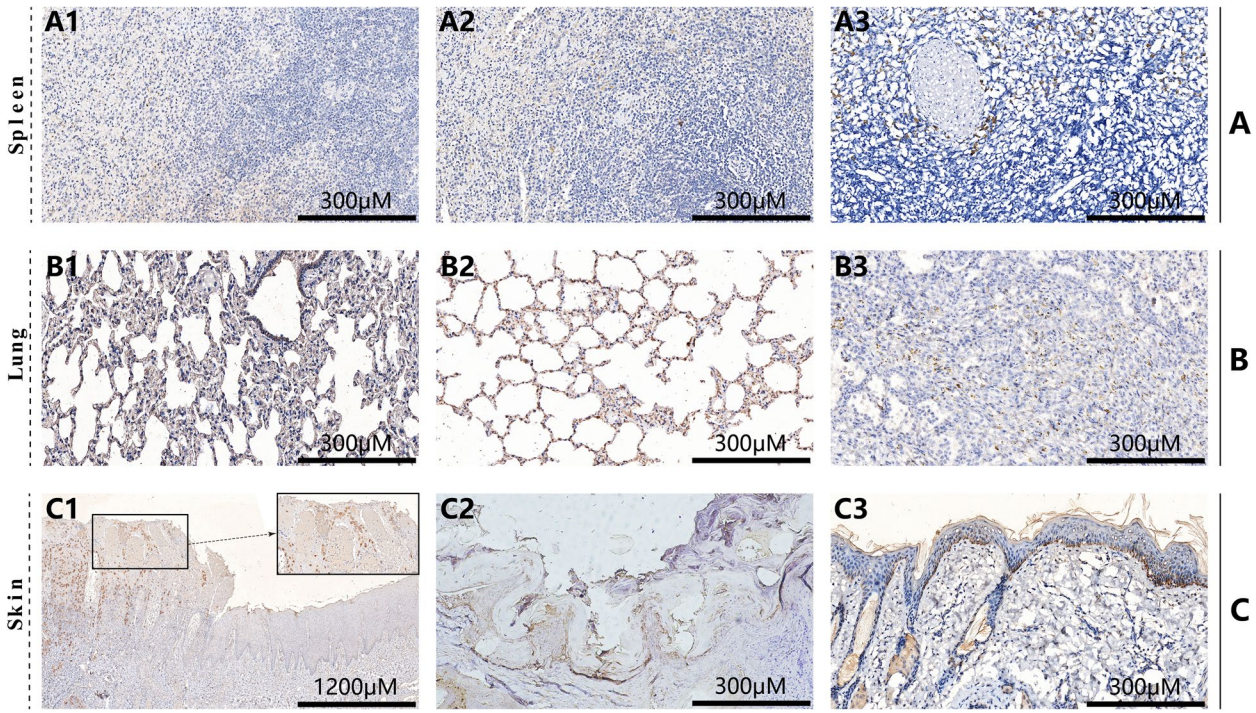

Fig. 5 Immunohistochemical detection of lumpy skin disease virus antigen in spleen, lung, and skin tissues. **A** Spleen section. **B** Lung section. **C** Skin section

Table 1 Serum biochemical profile of cattle A, highlighting hypoalbuminemia, hyperglobulinemia, elevated ALT, and low cholesterol relative to standard bovine reference intervals

Item	Result	Reference interval	Level
ALB (albumin)	2.4 g/dL	2.5–3.6 g/dL	Low
ALKP (alkaline Phosphatase)	24 U/L	10–149 U/L	Normal
ALT (alanine aminotransferase)	70 U/L	12–40 U/L	High
AMYL (amylase)	28 U/L	0–28 U/L	Normal
BUN (blood urea nitrogen)	8 mg/dL	7–17 mg/dL	Normal
CA (calcium)	8.9 mg/dL	7.8–10.5 mg/dL	Normal
CHOL (cholesterol)	27 mg/dL	76–227 mg/dL	Low
CREA (creatinine)	0.9 mg/dL	0–2 mg/dL	Normal
GGT (gamma-glutamyl transferase)	11 U/L	0–80 U/L	Normal
GLOB (globulin)	6.0 g/dL	2.7–3.8 g/dL	High
GLU (glucose)	73 mg/dL	46–93 mg/dL	Normal
LIPA (lipase)	115 U/L	30–400 U/L	Normal
PHOS (phosphorus)	5.5 mg/dL	4.3–7.9 mg/dL	Normal
TBIL (total bilirubin)	< 0.1 mg/dL	0–0.7 mg/dL	Normal
TP (total protein)	8.3 g/dL	5.8–8.0 g/dL	High
ALB/GLOB (albumin to globulin ratio)	0.4	—	—
BUN/CREA (blood urea nitrogen to creatinine ratio)	10	—	—

Table 2 Serum biochemical profile of cattle B, showing marked hypocholesterolemia, while all other parameters remained within bovine reference intervals

Item	Result	Reference interval	Level
ALB (albumin)	3.2 g/dL	2.5–3.6 g/dL	Normal
ALKP (alkaline phosphatase)	38 U/L	10–149 U/L	Normal
ALT (alanine aminotransferase)	15 U/L	12–40 U/L	Normal
AMYL (amylase)	< 5 U/L	0–28 U/L	Normal
BUN (blood urea nitrogen)	13 mg/dL	7–17 mg/dL	Normal
CA (calcium)	8.3 mg/dL	7.8–10.5 mg/dL	Normal
CHOL (cholesterol)	39 mg/dL	76–227 mg/dL	Low
CREA (creatinine)	1.7 mg/dL	0–2 mg/dL	Normal
GGT (gamma-glutamyl transferase)	18 U/L	0–80 U/L	Normal
GLOB (globulin)	3.8 g/dL	2.7–3.8 g/dL	Normal
GLU (glucose)	82 mg/dL	46–93 mg/dL	Normal
LIPA (lipase)	54 U/L	30–400 U/L	Normal
PHOS (phosphorus)	6.4 mg/dL	4.3–7.9 mg/dL	Normal
TBIL (total bilirubin)	< 0.1 mg/dL	0–0.7 mg/dL	Normal
TP (total protein)	7.0 g/dL	5.8–8.0 g/dL	Normal
ALB/GLOB (albumin to globulin ratio)	0.8	—	—
BUN/CREA (blood urea nitrogen to creatinine ratio)	7	—	—

(Table 2), affecting apolipoprotein synthesis before changes in transaminase activity or plasma protein levels occur. These findings highlight the varied liver responses to viruses causing lumpy skin disease and emphasize the importance of assessing plasma proteins, lipid fractions, and enzymes together for accurate disease staging.

Discussion

Since LSDV was first confirmed in China in 2019, it has spread across many provinces, reflecting a broader Asian trend. The current outbreak affects herds that have not been vaccinated, making them vulnerable. The long incubation period and nonspecific early symptoms make early detection difficult, necessitating laboratory tests

(Datten et al. 2023). Molecular detection has improved, with TaqMan-MGB real-time PCR offering ten times greater sensitivity than conventional PCR does, enabling quick identification of subclinical carriers (Nan et al. 2023). Serology based on the A33 envelope protein achieves nearly 99% diagnostic accuracy, enhancing outbreak screening (Chen et al. 2024). Histology and immunohistochemistry highlight angiotropic pathogenesis, with viral antigens concentrated in specific areas, which aligns with evidence that LSDV replicates in macrophage and dendritic niches (Haider et al. 2024). This endothelial preference explains the common occurrence of septal thrombi, mineralized arteriolar casts, and dermal vasculitis in tissue sections. Similar vasculopathy patterns were found in up to two-thirds of lung samples during recent Asian outbreaks (Şevik et al. 2016). Experimental data show that the virus first targets endothelial beds before spreading to the epithelium, matching the strong antigen presence in basal keratinocytes observed here (Bianchini et al. 2023). Ongoing endothelial activation also explains focal hepatic amyloid due to chronic serum amyloid-A buildup in slow-flow sinusoids (Şevik et al. 2016). Serum chemistry data support these findings, with low albumin, high globulin, and a low albumin–globulin ratio indicating a negative acute phase protein response and increased immunoglobulin production, which are linked to severe clinical outcomes (El-Mandrawy and Alam 2021). Elevated alanine aminotransferase without an increase in alkaline phosphatase suggests cytosolic leakage from inflamed liver cells rather than cholestasis (Kamr et al. 2022). Significant hypocholesterolemia, even with normal enzyme levels, supports findings that lipid synthesis is an early target of LSDV infection due to the suppression of hepatocyte nuclear factor 4α by interleukin-6 (Neamat-Allah 2015). Thus, decreasing cholesterol levels along with a lower albumin-to-globulin ratio can indicate subclinical liver involvement, aligning with known bovine protein diagnostics (McPherson and Pincus 2021). Vector exposure is the most likely way in which viruses are introduced, particularly during peak seasons for Culicoides midges and Stomoxys flies (Chihota et al. 2001). Preventive vaccination is key for controlling outbreaks in herds. Neethling strain live vaccines show greater than 90% efficacy and are more effective than heterologous Capri pox vaccines. Adjuvanted inactivated vaccines offer increased safety when live vaccines cannot be used. However, vaccination should be combined with strict vector control and a 14-day quarantine, including paired serology and PCR testing for new cattle (Riana et al. 2024; Agianniotaki et al. 2017; Islam et al. 2021). Currently, there is no approved antiviral treatment for LSDV, so supportive care is essential. Key measures include isolation, fluid replacement, vitamin supplementation, and careful wound care with povidone iodine and antibiotics to prevent bacterial infections (Tuppuraine et al. 2017; Toker et al. 2022; Zheng et al. 2021).

Herbal remedies may help heal lesions faster. These insights highlight the importance of endothelial damage in disease progression, the diagnostic benefits of molecular and serological tests, the prognostic value of ongoing biochemical monitoring, and the need for a comprehensive control strategy combining vaccination, vector control, and supportive care.

Conclusion

This case series shows that the lumpy skin disease virus primarily causes blood vessel-related damage, evident as lung nodules and widespread microthrombosis, with a biphasic immune response peaking around day 20. Strong immunohistochemical signals in the skin, lungs, and spleen highlight the diagnostic importance of PCR-ELISA testing and targeted tissue sampling. These findings suggest that endothelial injury is the main cause of systemic damage and emphasize the need for combined control measures, including vaccination, vector control, and supportive therapy, to reduce morbidity and economic loss.

Methods

Detection of antibody

Following venepuncture, blood specimens were allowed to clot at 22°C for 30 min and then centrifuged at 5000×*g* for 10 min to obtain clear serum. Serum aliquots (50 µL per well) were analyzed in duplicate with a commercial double antigen sandwich ELISA specific for capripoxvirus antibodies (ID Screen Capripox Multi-species, kit code CPVDA 0117; ID Vet, Grabels, France) according to the manufacturer's protocol. It's a positive result when S/P > 30%. Briefly, plates pre-coated with recombinant LSDV antigen were incubated with test sera for 45 min at 37°C, washed three times with PBS-Tween (0.05%), and further incubated for 30 min with horseradish-peroxidase-conjugated antigen (Yuan et al. 2024). After a final wash, tetramethyl-benzidine substrate was added; the enzymatic reaction was stopped after 15 min with 0.5 M sulfuric acid, and optical density (OD) was measured at 450 nm using a calibrated microplate reader. Each run included kit-supplied positive and negative controls plus an internal low-positive control derived from previously confirmed field sera, as recommended by the WOAH Terrestrial Manual. Results were expressed as sample to positive (S/P) ratios; samples with S/P ≥ 30% were considered seropositive per kit validation data, which show diagnostic sensitivity of 95% and specificity of 98%.

Residual sera were aliquoted and stored at −80°C for confirmatory virus neutralization testing and future longitudinal studies.

Histopathology (H&E staining)

Paraformaldehyde-fixed tissue blocks were trimmed into 1 cm×1 cm cross-sectional specimens. Following sequential dehydration through a graded ethanol series, tissues were cleared in xylene and embedded in paraffin wax. Sectioning was performed at a thickness of 3–5 μm using a rotary microtome, with samples mounted on adhesive coated slides and dried at 60°C. Deparaffinization was achieved through immersion in xylene, followed by rehydration via a descending ethanol gradient to distilled water. Nuclear staining was performed with Mayer's hematoxylin, differentiated in 1% acid alcohol, blued in Scott's tap water substitute, and counterstained with eosin Y. Finalized sections were dehydrated through ascending ethanol, cleared in xylene, and permanently mounted with neutral balsam.

Immunohistochemistry

Post-standard H&E preprocessing, antigen retrieval was performed using citrate buffer to unmask epitopes. Endogenous peroxidase activity was quenched with 3% H_2O_2, followed by blocking with 5% normal goat serum for 1 h. (The primary antibody was applied under optimized conditions LSDV clinically positive serum was diluted at 1:8,000 and used as the primary antibody, with serum from healthy cattle serving as the negative control.) After PBS-T washing, the HRP-conjugated secondary antibody was incubated. The DAB chromogen was microscopically monitored until an optimal signal development was achieved. Counterstaining with modified hematoxylin was performed before final dehydration and mounting. A semi-quantitative scoring system was applied based on the percentage of positive cells and staining intensity (Li et al. 2015).

PCR detection of LSDV DNA

PCR was performed with primers designed to GB/T 39602–2020 (Forward 5′-CCTCCTTTTAAGCTACTTTTTCTTA-3′; Reverse 5′-GATACATGTAGGAACATTGTTACCTA-3′). Cycling: 95℃ 5 min; 35×(95℃ 30 s, 52℃ 30 s, 72℃ 30 s); final extension 72℃ 5 min.

Serum biochemistry

For biochemical profiling, whole blood samples collected in heparinized anticoagulant tubes were centrifuged at 5,000×*g* for 10 min at 4°C. A 300 μL aliquot of the supernatant serum was transferred to standardized assay cuvettes, and 17 biochemical parameters were quantitatively analyzed using an IDEXX VetTest 8008 biochemical analyzer. All procedures were conducted in accordance with the Institutional Animal Care Committee's guidelines.

Data analysis and presentation

The dataset consisted of 19 ELISA measurements collected from 16 unique animals across three farms. Due to the opportunistic sampling during outbreaks, this constituted an unbalanced longitudinal dataset: 13 animals were sampled only once (providing cross-sectional data), while three animals were sampled at two time points (providing longitudinal data). Given the sample size and structure, the analysis was strictly descriptive and focused on individual-level data. No group means or confidence intervals were calculated. Data are presented in scatter plots where: Each symbol represents a single ELISA measurement. Symbols are colored and shaped by farm of origin. Lines connect sequential measurements from the same individual animal to visualize within-animal kinetics. All data visualization was performed using GraphPad Prism V. 8.0.

Abbreviations

PCR	Polymerase Chain Reaction
ELISA	Enzyme-Linked Immunosorbent Assay
LSD	Lumpy skin disease
LSDV	Lumpy skin disease virus
GTPV	Goat pox virus
SPPV	Sheep pox virus

Supplementary Information

The online version contains supplementary material available at https://doi.org/10.1186/s44149-025-00205-7.

Supplementary material Figure S1. Clinical symptoms of this LSDV patient. Figure S2. (A) PCR analysis of the clinical samples. (B) Changes in the antibody levels detected via ELISA. Figure S3. Gross anatomical observations of organs and tissues from LSD-affected cattle. Figure S4. HE staining results of the liver, lungs, kidneys and cutaneous nodules. Figure S5. Results of immunohistochemical staining of pulmonary, splenic and cutaneous nodules. Figures S1-3. IHC negetive control for lung, skin and spleen.

Acknowledgements

We extend our sincere gratitude to the College of Veterinary Medicine, Huazhong Agricultural University, for providing the experimental platform.

Authors' contributions

HCM and ZJH conceived and designed the experiments. KL, QX, DYT, SXH, JMX, JCH, ZEP, WZY, SL, YXW, and JWF collected the clinical samples, and JWF and ZJH performed the experiments and analyzed the data. ZJH wrote the manuscript. HCM, GAZ, and GJD checked and finalized the manuscript. All the authors have read and approved the final version of the manuscript.

Funding

This study was funded by the National Key Research and Development Program of China (#2022YFD1800701), The LIJIANG Joint Expert Studio of Guo Aizhen, Zhang Meiyan and Li Weijuan (20233335C02) and the Chinese Agricultural Research System of MOF and MARA (#CARS-37).

Data availability
All the data generated and analyzed during this study are included in the main manuscript or supplementary materials/files.

Declarations

Ethics approval and consent to participate
This study was conducted in strict accordance with the recommendations provided in the Guide for the Care and Use of Laboratory Animals of the Ministry of Science and Technology of the People's Republic of China. The animal experiments were approved by the Hubei Administrative Committee for Laboratory Animals (Approval Number: HZAUCA-2025-0056). The animal autopsy procedures and related experimental procedures described in this manuscript were conducted with the written consent of the animal owner. Clinical sample collection was conducted in strict accordance with aseptic procedures and was performed with the prior consent of the cattle farm owner.

Consent for publication
Not applicable.

Competing interests
The authors declare that they have no conflicts of interest.

Received: 25 August 2025 Accepted: 27 October 2025
Published online: 06 January 2026

References

Agianniotaki, E. I., E. Mathijs, F. Vandenbussche, K. E. Tasioudi, A. Haegeman, P. Iliadou, S. C. Chaintoutis, C. I. Dovas, S. Van Borm, E. D. Chondrokouki, et al. 2017. Complete genome sequence of the lumpy skin disease virus isolated from the first reported case in Greece in 2015. *Genome Announcements* 5 (29): e00550-e617. https://doi.org/10.1128/genomeA.00550-17.

Ayelet, G., Y. Abate, T. Sisay, H. Nigussie, E. Gelaye, S. Jemberie, and K. Asmare. 2013. Lumpy skin disease: Preliminary vaccine efficacy assessment and overview on outbreak impact in dairy cattle at Debre Zeit, central Ethiopia. *Antiviral Research* 98 (1): 261–265. https://doi.org/10.1016/j.antiviral.2013.02.008.

Bianchini, J., X. Simons, M.F. Humblet, and C. Saegerman. 2023. Lumpy skin disease: A systematic review of mode of transmission, risk of emergence and risk entry pathway. *Viruses* 15 (8): 1622. https://doi.org/10.3390/v15081622.

Chen, G., X. He, Z. Gao, Y. Fang, T. T. Hurisa, H. Jia, J. Tan, G. Zhou, B. Fu, W. Li, et al. 2024. Development of a competitive ELISA based on the LSDV A33 antigen. *Virology Journal* 21 (1): 203. https://doi.org/10.1186/s12985-024-02448-1.

Chihota, C. M., L. F. Rennie, R. P. Kitching, and P. S. Mellor. 2001. Mechanical transmission of lumpy skin disease virus by *Aedes aegypti* (Diptera: Culicidae). *Epidemiology and Infection* 126 (2): 317–321. https://doi.org/10.1017/s0950268801005179.

Datten, B., A. A. Chaudhary, S. Sharma, L. Singh, K. D. Rawat, M. S. Ashraf, L. M. Alneghery, M. O. Aladwani, H. A. Rudayni, D. Dayal, et al. 2023. An extensive examination of the warning signs, symptoms, diagnosis, available therapies, and prognosis for lumpy skin disease. *Viruses* 15 (3): 604. https://doi.org/10.3390/v15030604.

Davies, F. G. 1976. Characteristics of a virus causing a pox disease in sheep and goats in Kenya, with observation on the epidemiology and control. *Journal of Hygiene* 76 (2): 163–171. https://doi.org/10.1017/s0022172400055066.

El-Mandrawy, Shefaa A. M., and Rasha T. M. Alam. 2021. Hematological, biochemical and oxidative stress studies of lumpy skin disease virus infection in cattle. *Journal of Applied Animal Research* 46 (1): 1073–1077. https://doi.org/10.1080/09712119.2018.1461629.

Flannery, J., B. Shih, I. R. Haga, M. Ashby, A. Corla, S. King, G. Freimanis, N. Polo, A. C. Tse, C. J. Brackman, et al. 2021. A novel strain of lumpy skin disease virus causes clinical disease in cattle in Hong Kong. *Transboundary and Emerging Diseases* 69 (4): e336-343. https://doi.org/10.1111/tbed.14304.

Haider, A., Z. Abbas, A. Taqveem, A. Ali, M. Khurshid, R. .F. . El. Naggar, M. A. Rohaim, and M. Munir. 2024. Lumpy skin disease: Insights into molecular pathogenesis and control strategies. *Veterinary Sciences* 11 (11): 561. https://doi.org/10.3390/vetsci11110561.

Islam, S. J., C. Deka, and P. J. Sonowal. 2021. Treatment and management of lumpy skin disease in cow: A case report. *International Journal of Veterinary Sciences and Animal Husbandry* 6 (2): 26–27. https://doi.org/10.22271/veterinary.2021.v6.i2a.331.

Kamr, A., H. Hassan, R. Toribio, A. Anis, M. Nayel, and A. Arbaga. 2022. Oxidative stress, biochemical, and histopathological changes associated with acute lumpy skin disease in cattle. *Veterinary World* 15 (8): 1916–1923. https://doi.org/10.14202/vetworld.2022.1916-1923.

Li, Y. X., Zhang, L., Simayi, D., Zhang, N., Tao, L., Yang, L., Zhao, J., Chen, Y. Z., Li, F., Zhang, W. J. 2015. Human Papillomavirus Infection Correlates with Inflammatory Stat3 Signaling Activity and IL-17 Level in Patients with Colorectal Cancer. *PLoS ONE*. 10(2):e0118391. https://doi.org/10.1371/journal.pone.0118391.

Nan, W., Gong, M., Lu, Y., Li, J., Li, L., Qu, H., Liu, C., Wang, Y., Wu, F., Wu, X. et al. 2023. A novel triplex real-time PCR assay for the differentiation of lumpy skin disease virus, goatpox virus, and sheeppox virus. *Frontiers in Veterinary Science* 10:1175391. https://doi.org/10.3389/fvets.2023.1175391.

Neamat-Allah, A.N.F. 2015. Immunological, hematological, biochemical, and histopathological studies on cows naturally infected with lumpy skin disease. *Vet World* 8 (9): 1131–1136. https://doi.org/10.14202/vetworld.2015.1131-1136.

Parvin, R., Chowdhury, E.H., Islam, M.T., Begum, J. A., Nooruzzaman, M., Globig, A., Dietze, K., Hoffmann, B. and Tuppurainen, E. 2022. Clinical epidemiology, pathology, and molecular investigation of lumpy skin disease outbreaks in Bangladesh during 2020–2021 indicate the re-emergence of an old African strain. *Viruses* 14 (11): 2529. https://doi.org/10.3390/v14112529.

Riana, E., C. Sri-In, T. Songkasupa, L. C. Bartholomay, A. Thontiravong, and S. Tiawsirisup. 2024. Infection, dissemination, and transmission of lumpy skin disease virus in *Aedes aegypti* (Linnaeus), *Culex tritaeniorhynchus* (Giles), and *Culex quinquefasciatus* (Say) mosquitoes. *Acta Tropica* 254:107205. https://doi.org/10.1016/j.actatropica.2024.107205.

Richard A. McPherson, Matthew R. Pincus. 2022. Henry's clinical diagnosis and management by laboratory methods (24th ed.). Elsevier. ISBN: 9780323673204

Sariya, L., W. Paungpin, S. Chaiwattanarungruengpaisan, M. Thongdee, C. Nakthong, A. Jitwongwai, S. Taksinoros, K. Sutummaporn, S. Boonmasawai, and B. Kornmatitsuk. 2022. Molecular detection and characterization of lumpy skin disease viruses from outbreaks in Thailand in 2021. *Transboundary and Emerging Diseases* 69 (5): e2145-2152. https://doi.org/10.1111/tbed.14552.

Sendow, I., I. K. Meki, N. L. P. I. Dharmayanti, H. Hoerudin, A. Ratnawati, T. B. K. Settypalli, H. O. Ahmed, H. Nuradji, M. Saepulloh, R. S. Adji, et al. 2024. Molecular characterization of recombinant LSDV isolates from 2022 outbreak in Indonesia through phylogenetic networks and whole-genome SNP-based analysis. *BMC Genomics* 25 (1): 240. https://doi.org/10.1186/s12864-024-10169-6.

Şevik, M., O. Avci, M. Doğan, and Ö. B. İnce. 2016. Serum biochemistry of lumpy skin disease virus-infected cattle. *BioMed Research International* 2016:6257984. https://doi.org/10.1155/2016/6257984.

Shumilova, I., A. Krotova, A. Nesterov, O. Byadovskaya, A. van Schalkwyk, and A. Sprygin. 2022. Overwintering of recombinant lumpy skin disease virus in northern latitudes, Russia. *Transboundary and Emerging Diseases* 69 (5): e3239-3243. https://doi.org/10.1111/tbed.14521.

Sprygin, A., T. Sainnokhoi, D. Gombo-Ochir, T. Tserenchimed, A. Tsolmon, O. Byadovskaya, U. Ankhanbaatar, A. Mazloum, F. Korennoy, and I. Chvala. 2022. Genetic characterization and epidemiological analysis of the first lumpy skin disease virus outbreak in Mongolia, 2021. *Transboundary and Emerging Diseases* 69 (6): 3664–3672. https://doi.org/10.1111/tbed.14736.

Toker, Eda Baldan, Ozer Ates, and Kadir Yeşilbağ. 2022. Inhibition of bovine and ovine capripoxviruses (lumpy skin disease virus and sheeppox virus) by ivermectin occurs at different stages of propagation in vitro. *Virus Research* 310:198671. https://doi.org/10.1016/j.virusres.2021.198671.

Tuppuraine, E. S., T. Alexandrov, and D. Beltran-Alcrudo. 2017. Lumpy skin disease field manual: A manual for veterinarians. *FAO Animal Production Health Manual* 20:1–60.

Tuppurainen, E. S. M., C. R. Pearson, K. Bachanek-Bankowska, N. J. Knowles, S. Amareen, L. Frost, M. R. Henstock, C. E. Lamien, A. Diallo, and P. P. C. Mertens. 2014. Characterization of sheep pox virus vaccine for cattle

against lumpy skin disease virus. *Antiviral Research* 109:1–6. https://doi.org/10.1016/j.antiviral.2014.06.009.

Van Borm, S., S. Dellicour, D. P. Martin, P. Lemey, E. I. Agianniotaki, E. D. Chondrokouki, D. Vidanovic, N. Vaskovic, T. Petrović, S. Lazić, et al. 2023. Complete genome reconstruction of the global and European regional dispersal history of the lumpy skin disease virus. *Journal of Virology* 97 (11): e0139423–e0139423. https://doi.org/10.1128/jvi.01394-23.

Wang, J., Z. Xu, Z. Wang, Q. Li, X. Liang, S. Ye, K. Cheng, L. Xu, J. Mao, Z. Wang, et al. 2022. Isolation, identification and phylogenetic analysis of lumpy skin disease virus strain of outbreak in Guangdong, China. *Transboundary and Emerging Diseases* 69 (5): e2291-2301. https://doi.org/10.1111/tbed.14570.

Yuan, X. W., H. Zhao, W. F. Ji, X. H. Yan, Z. J. Xiang, L. Yang, Y. C. Geng, Y. Y. Chen, J. G. Chen, X. et al. 2024. Preparation of a monoclonal antibody against recombinant LSDV034 protein and its application in detecting lumpy skin disease virus through a competitive enzyme-linked immunosorbent assay (cELISA). *Animal Diseases* 4:23. https://doi.org/10.1186/s44149-024-00126-x.

Zheng, W., Y. Luping, Q. Yidan, and W. Yu. 2021. Progress in pathophysiology and integrated traditional Chinese and Western medicine of postintensive care syndrome. *Chinese Critical Care Medicine* 33 (2): 252–256. https://doi.org/10.3760/cma.j.cn121430-20201102-00699.

Publisher's Note